JOURNAL OF MATERIALS SCIENCE 18 (1983) 1306–1314

Dynamic fatigue of brittle materials containing indentation line flaws

BETH L. SYMONDS, R. F. COOK
Department of Applied Physics, School of Physics, University of New South Wales, Kensington, NSW 2033, Australia

B. R. LAWN
Fracture and Deformation Division, National Bureau of Standards, Washington, DC 20234, USA

A study is made of the dynamic fatigue response of brittle materials containing indentation-induced line flaws. The theoretical fracture mechanics of "median" crack evolution to failure under applied tension are first developed, with special emphasis on the role of residual contact stresses. In particular, it is shown that use of fatigue curves to evaluate the exponent in an assumed power-law crack velocity function may result in systematic error, by as much as a factor of two, if proper account is not taken of this residual contact contribution. Data from strength tests on soda-lime glass bars in water, using a tungsten carbide cutting wheel to introduce the median pre-cracks, confirm the basic predictions. The results suggest that extreme care needs to be exercised when using surfaces with a contact history, e.g. as with machining damage, in fatigue test programmes for materials analysis.

1. Introduction

In a series of recent papers it has been shown how controlled indentation flaws can be used to obtain accurate and reliable fatigue strength data for brittle materials [1–6]. The capacity to predetermine the scale and location of the critical flaw is a key element in the fracture mechanics analysis, for the experimenter then has the unique opportunity of following the flaw at all stages of its evolution to failure. A major conclusion which emerges from such observations is that the Griffith concept of a well-defined microcrack driven exclusively by an applied tensile field is inadequate; the indentation flaw certainly does have the nature of a well-defined crack, but its driving force contains an important additional component, one associated with the residual stress field about the plastic contact zone [7–9]. The influence of this additional component is manifest in conventional fatigue plots, i.e. in plots of failure stress against stress rate ("dynamic fatigue") [1] or lifetime ("static fatigue") [2]. Thus whereas for flaws satisfying a power-law crack velocity function the linearity of such plots in logarithmic coordinates still holds to good approximation, the slope and intercept are significantly altered. The "apparent" exponent and coefficient of this velocity function evaluated from fatigue data need to be converted, via an appropriate set of "transformation equations" [3–6], to "true" parameters representative of macroscopic crack growth.

Although indentation crack systems might appear as somewhat contrived entities in the context of the strength of real materials, there is increasing evidence to suggest that such systems do, in many important practical cases, contain the essence of flaw response. This is especially so for flaws with a surface-contact history, e.g. particle impact [10, 11], where the analogy with an indentation process is obvious; however, insofar as the distinctive feature of the flaw description is the presence of a residual crack driving force, the modified fatigue analysis may have a far broader compass than this [6]. On the

0022–2461/83 $03.00 + .12

other hand, the analysis developed in the earlier studies [1–5] was restrictive in one important sense, that of flaw geometry; by considering only axisymmetric indentations, e.g. as produced by a normally loaded Vickers pyramid, the transformation relations derived were strictly applicable to just "point" flaw configurations. "Line" flaw configurations, e.g. as produced by translating a sharp indenter across a surface [12], are governed by different starting equations in the fracture mechanics formulation. In the most recent of the fatigue studies Fuller *et al.* [6] analysed the two geometrical types in some detail, and concluded that the line flaw was even more sensitive to residual-stress effects than its point-flaw counterpart. In particular, whereas for the latter case the apparent and true crack velocity exponents differed by a factor of about 4/3, for the former the corresponding factor was about 2. Discrepancies of this magnitude have indeed been reported by Pletka and Wiederhorn [13] in fatigue tests on surface-machined ceramics, although in their experiments no attempt was made to characterize the critical flaw.

In this paper we present the results of an experimental study of controlled line flaws aimed at testing the predictions of the residual stress theory. The test material is the same soda-lime glass as used in earlier work [1, 2], thereby providing a convenient base for data comparison. Line flaws are introduced by means of a glass-cutting wheel [14]. The failure tests are conducted at constant stressing rates in water. Analysis of the ensuing fatigue plot confirms the existence of a large discrepancy in the velocity exponents. It is concluded that extreme care needs to be exercised in the use of strength data from "natural" surfaces in the evaluation of materials for long-lifetime applications.

2. Theoretical background

Consider the line flaw system shown in Fig. 1. The contact event responsible for creating the flaw is characterized by the residual deformation track, half-width a, that it leaves on the specimen surface. There are two main ways in which such a track may be produced: (i) in wedge loading at normal force P_l per unit length along the contact line; (ii) in axisymmetric loading at normal force P, but with linear translation. Of these, the second, the case illustrated in Fig. 1, is more amenable to controlled experimentation, although it can be

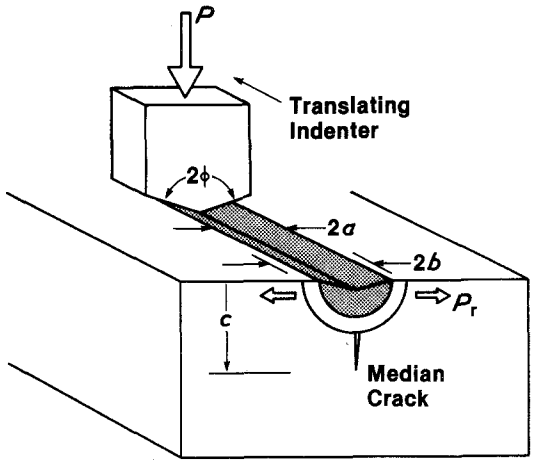

Figure 1 Schematic showing parameters of line flaw system.

argued that there is a certain equivalence between the two (Appendix I). Immediately below the deformation track a "median" crack, depth c, is formed. This crack leaves no characteristic "radial" trace on the specimen surface, as it does with point indentations [9]. In general, sideways-spreading "lateral" cracks (not shown in Fig. 1) also form below the deformation track [12]; these play only a secondary role in the strength degradation process, and will accordingly not be given detailed attention here.

The line flaw system thus produced is subjected to a subsequent applied tensile stress σ_a, which takes the median crack system to failure. The object of our exercise here is to determine the critical failure stress, σ_f, under dynamic fatigue conditions, i.e. $\dot{\sigma}_a$ = constant, in terms of appropriate indentation variables and crack velocity parameters.

2.1. Incorporation of residual contact term into basic fracture mechanics

In this section we write down a stress intensity factor for the line flaw configuration, placing special emphasis on the residual contact component. We also derive expressions for the "inert" strength to provide a reference baseline for analysis of the ensuing fatigue response.

Regardless of the way in which the linear deformation track is produced there will be a residual stress field of approximately cylindrical symmetry due to elastic/plastic mismatch. The source of this field lies in the accommodation of the contact impression volume by the elastic

matrix surrounding the plastic zone radius b [9]. A detailed analysis of the field intensity in terms of the elastic/plastic properties of the test material and the characteristic half-angle ϕ of the indenter is given in Appendix II. For present purposes it is sufficient to define a single, dimensionless material/indenter parameter χ which incorporates all these factors into a simple expression for the residual driving force on the median crack. Thus we may write a residual stress intensity factor of the general form for straight cracks generated by an "effective" line force P_l [12],

$$K_r = \chi P_l / c^{1/2}. \quad (1)$$

For static line loading P_l identifies with the *actual* line force on the indenter; for translating point loading we may talk of an *equivalent* line force (Appendix I). (It may be noted that the corresponding stress intensity factor for statically loaded point flaws differs only in the crack-size exponent, 3/2 instead of 1/2 [8].)

If the residual stress factor in Equation 1 were to be sufficient to maintain the median crack in a state of mechanical equilibrium after completion of the contact process, i.e. $K = K_c$, where K_c defines the material toughness, then

$$c_0 = (\chi P_l / K_c)^2 \quad (2)$$

would represent the initial crack depth in the subsequent strength testing. There are, however, several factors which effectively relax K_r below K_c, in which case Equation 2 underestimates the true crack depth, c_0' say. First, during the actual contact process there is an elastic component of the field which augments the residual component [7, 9]. Whereas for a line contact this component is zero at the median plane, for a point contact it is tensile [15]. In the latter case, therefore, the maximum crack driving force is attained at full loading, so that the crack must close up partially as the indenter is withdrawn. Second, the growth of lateral cracks, which tends to occur also upon indenter withdrawal, can relax the intensity of the residual field somewhat [1, 14, 16]. Third, the presence of a reactive environment can cause post-indentation, subcritical extension of the median crack [1, 17]. Clearly, the degree to which Equation 2 underestimates the initial crack depth in the failure test will depend on the elastic/plastic properties of the material, but other factors, such as the exposure time of the indented surface to the atmosphere, can have a significant effect.

Suppose now the median crack is subjected to the tensile stress σ_a. The stress intensity factor appropriate to this loading is of the familiar form

$$K_a = \psi \sigma_a c^{1/2} \quad (3)$$

where ψ is a crack geometry constant. Equations 1 and 3 may then be combined additively to yield the net stress intensity factor

$$K = K_r + K_a = \chi P_l / c^{1/2} + \psi \sigma_a c^{1/2}, \quad (c \geqslant c_0'). \quad (4)$$

The strength of the test piece is determined as the stress to take the crack from its initial size to an instability configuration, defined by the condition $K = K_c$, $dK/dc > 0$.

The strength under inert conditions of testing can be obtained immediately from Equation 4 by requiring that the crack should remain in a state of mechanical equilibrium in its approach to the instability. Accordingly, we insert $K = K_c$ into Equation 4, and rearrange to determine the equilibrium-stress/crack-size function

$$\sigma_a = (K_c / \psi c^{1/2})(1 - \chi P_l / K_c c^{1/2}). \quad (5)$$

For the limiting case $\chi = 0$, corresponding to ideal Griffith flaws, the failure is spontaneous at the initial flaw size, so the inert strength at $\sigma_i^0 = \sigma_a(c_0')$ is given by

$$\sigma_i^0 = K_c / \psi c_0'^{1/2} \quad (6)$$

in the absence of residual stresses.

For the more general case $\chi \neq 0$, the failure mechanics are more complex [8]. The function $\sigma_a(c)$ in Equation 5 now passes through a maximum at

$$c_m = (2\chi P_l / K_c)^2 \quad (7)$$

and the failure condition is contingent on whether c_0' is smaller or larger than this quantity. If smaller, the flaw must undergo a stage of stable, precursor crack growth prior to the critical instability. It is noted that c_m in Equation 7 exceeds c_0 in Equation 2 by a factor of 4; recalling that $c_0 \leqslant c_0'$ always, this factor represents the maximum degree of precursor extension possible. (We may note that the ratio c_m/c_0 for line flaws is substantially larger than that for point flaws [6, 8], namely, 2.52, reflecting a less rapid falloff in the function $K(c)$ in the former instance.) Insertion of Equation 7 back into Equation 5 gives the appropriate inert strength at $\sigma_i = \sigma_a(c_m) = \sigma_m$, i.e.

$$\sigma_i = K_c/2\psi c_m^{1/2} = K_c^2/4\psi\chi P_l, \quad (c_0' \leqslant c_m). \tag{8a}$$

If, on the other hand, c_0' is larger than c_m, the crack becomes critical without precursor extension; insertion of $\sigma_i = \sigma_a(c_0')$ into Equation 5 accordingly yields

$$\sigma_i = (K_c/\psi c_0'^{1/2})(1 - \chi P_l/K_c c_0'^{1/2}), \quad (c_0' > c_m). \tag{8b}$$

We note that the inital flaw size appears explicitly only in the second of these last two equations.

2.2. Dynamic fatigue formalism

In keeping with our previous course [1–6] we assume that in a reactive chemical environment the median crack can grow subcritically, i.e. at $K < K_c$, in accordance with the crack velocity function

$$v = v_0(K/K_c)^n \tag{9}$$

where the exponent n and coefficient v_0 are parameters to be determined empirically for any given material/environment system. In combination with Equation 4 this function yields, for a time-varying applied stress function $\sigma_a(t)$, a master differential equation for fatigue,

$$dc/dt = v_0[\chi P_l/K_c c^{1/2} + \psi\sigma_a(t)c^{1/2}/K_c]^n. \tag{10}$$

This equation has to be solved for the time to take the crack from its initial (stable) to its final (unstable) configuration, at which point the stress level defines the fatigue strength, $\sigma_a = \sigma_f$.

An analytical solution of Equation 10 is available only for the special case σ_a = constant = σ_f, with flaws in the precursor growth domain $c_0' \ll c_m$ [6]. However, this solution is of precisely the same form as obtained generally for Griffith-like flaws; there the effect of varying the function $\sigma_a(t)$ is manifest as a systematic change in the intercept of the appropriate (logarithmic) fatigue plot. On the assumption that the same generality holds for flaws with residual stress fields, we obtain the following result for the case of special interest here, namely $\dot{\sigma}_a = \sigma_a/t$ = constant = σ_f/t_f at specified contact load P_l [6]:

$$\sigma_f = (\lambda'\dot{\sigma}_a)^{1/(n'+1)} \tag{11}$$

where the slope on a plot of log σ_f against log $\dot{\sigma}_a$ relates to the true crack velocity exponent via the relation

$$n = 2n' - 2 \tag{12}$$

(cf. the case of Griffith flaws, for which $n = n'$); the intercept likewise relates to the velocity coefficient via

$$v_0 = (4\pi n')^{1/2}\sigma_m^{n'}c_m/\lambda'. \tag{13}$$

The validity of the generality assumption leading to this solution has been confirmed by numerical integrations of the master differential equation [3, 6].

Numerical analysis is also useful for investigating the effect of a varying initial flaw size on the fatigue behaviour [3]. Basically, it is found that the predicted $\sigma_f(\dot{\sigma}_a)$ response is insensitive to the value of c_0', up to c_m; beyond this point Equations 12 and 13 can no longer be relied upon to provide accurate crack velocity parameters. In the latter case, therefore, the advantage of a closed-form solution is lost, in addition to which additional, quantitative information on the initial crack condition is required. Notwithstanding these potential complications, Equation 12 serves to demonstrate the substantial discrepancies that can occur between "apparent" crack velocity parameters (i.e. as evaluated on the basis of zero residual stress) and "true" parameters pertinent to macroscopic crack laws.

3. Experimental

3.1. Procedure

Specimens of soda-lime glass, from the same batch as that used for the point-flaw studies of [1] and [2], were cut into bars 50 by 10 by 3 mm. These bars were annealed at 520° C for two days to remove any spurious surface stresses.

Line flaws were introduced along the transverse centre line of each prospective tensile surface for flexural strength testing. This was effected by mounting a bevelled tungsten carbide glass-cutting wheel of half-angle 66° and radius 3 mm onto the indenter arm of a standard hardness tester, allowing the wheel to bear down onto the specimen surface at a prescribed normal load, and translating the specimen support table at a velocity $\approx 0.5\,\text{mm sec}^{-1}$. The wheel traverse was stopped at a distance about 2 mm from opposite bounding faces of the specimen centre line, to avoid spurious edge chipping. The flaws thus produced were examined optically to ensure that the deformation tracks (see Appendix I) and the associated median cracks were sufficiently well defined. The flaws showed substantial birefringence in polarized light, consistent with the existence of an intense residual

contact field; an example is shown in Fig. 2. It was noted that at loads in excess of $P \approx 20$ N lateral crack growth became excessive to the point of causing occasional chipping. A normal load $P = 5$ N was thereby selected for all subsequent strength testing.

The strength tests themselves were conducted in four-point bending, with an outer span of 30.0 mm and an inner span of 7.0 mm. These were run about 30 min after indentation, to allow for saturation of post-contact slow crack growth (Section 2.1). Immediately prior to insertion into the bending fixture the indentation tracks were covered with either silicone oil, for inert strength testing, or water, for fatigue strength testing. The bending load delivered to the specimens was measured by a conventional strain-gauge instrumented cell for "slow" tests, i.e. for failure times > 10 sec, and by a piezoelectric cell for "fast" tests. Simple beam theory was used to evaluate the corresponding tensile stress on the flaw. All broken specimens were examined optically to confirm that failure had indeed initiated from the indentation site; those few exceptions, traceable to unusually large edge flaws, were rejected from the data accumulation.

3.2. Calibration tests

Some preliminary tests were carried out to investigate further the relative values of c_0' and c_m, bearing in mind the significant changes in the mechanical response of the crack system that are predicted once the former exceeds the latter (Sections 2.1 and 2.2). These tests also served to provide useful "calibration" parameters for the ensuing dynamic fatigue data analysis.

Accordingly, dummy specimens were prepared for crack depth measurements by section viewing. The sections were obtained by propagating large cracks from indentations on faces opposite to those containing the line flaws. This was most conveniently effected by stressing the specimens to failure in the bend apparatus, with the line flaws on the compression side to ensure no spurious extension of the primary crack system. An advantage of this procedure was that several line flaws could be placed on a given specimen. From 8 such flaws produced at the standard contact load of $P = 5$ N an initial flaw size $c_0' = 46 \pm 5\ \mu$m (mean and standard deviation) was measured.

In principle, a similar procedure could be used to gain an estimate of c_m, for systems in the domain $c_m > c_0'$. The method, successfully employed in an earlier study of point-indentation flaws [8], requires only that the crack system should be stressed to just below the critical instability prior to sectioning. However, comparative inert strength measurements for specimens with line flaws in the standard as-produced ($\chi \neq 0$) and re-annealed ($\chi = 0$) states [1] suggested that the condition $c_m > c_0'$ would be violated, thereby rendering this procedure ineffective. Thus, we obtained $\sigma_i = 81.0 \pm 9.5$ MPa and $\sigma_i^0 = 112.7 \pm 13.1$ MPa, respectively (mean and standard deviation, 10 specimens each series), corresponding to a ratio $\sigma_i/\sigma_i^0 = 0.72 \pm 0.17$. From Equations 6 to 8 we derive

$$c_m/c_0' = (\sigma_i^0/\sigma_i)^2/4, \qquad (c_0' \leqslant c_m) \tag{14a}$$

$$c_m/c_0' = 4(1 - \sigma_i/\sigma_i^0)^2, \qquad (c_0' > c_m) \tag{14b}$$

which gives us $c_m/c_0' = 0.31 \pm 0.24$; the line flaw system thus lies well outside the region where the fracture mechanics response is independent of initial conditions.

Figure 2 Section view of a linear flaw in glass, in crossed polars.

For the above determinations we may make two useful parameter evaluations. First, Equation 6 yields

$$\psi/K_c = 1/\sigma_i^0 c_0'^{1/2} = 1.31 \pm 0.17\ \mathrm{MPa}^{-1}\mathrm{m}^{-1/2}. \quad (15)$$

Then, in conjunction with Equation 8b, we obtain

$$\chi P_l/K_c = c_0'^{1/2}(1 - \sigma_i/\sigma_i^0) = (1.90 \pm 0.81) \times 10^{-3}\mathrm{m}^{1/2}. \quad (16)$$

4. Dynamic fatigue: results and analysis

The results of the dynamic fatigue tests are shown in Fig. 3. Each data point on this plot represents the mean and standard deviation, in logarithmic coordinates, of 10 to 15 specimens at the appropriate stress rate. The curve represents a numerical evaluation of the master differential equation, Equation 10, using the following parameters: ψ/K_c and $\chi P_l/K_c$, and the initial crack size c_0', as determined in Section 3.2; kinetic parameters $n = 17.9$ (± 0.5) and $v_0 = 2.4$ (± 0.6) mm sec^{-1} from the earlier study on the same glass/water system, but with re-annealed point flaws [1]. In comparing this curve with the data it should be noted that the evaluation of Equation 10 is sensitive to parameter input in the region $c_0' > c_m$; the large error quoted above for c_m/c_0' is especially pertinent in this context. With due acknowledgement of this point, we have been able to predict, to within the limits of experimental uncertainty, the fatigue response of specimens with contact-induced line flaws.

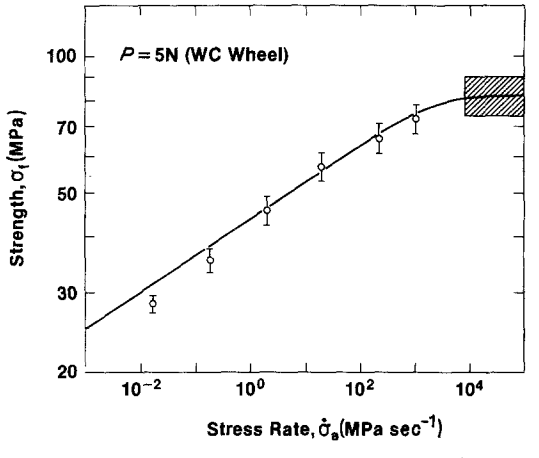

Figure 3 Dynamic fatigue of line-indented soda-lime glass in water. Curve through the data points represents evaluation of master differential equation, Equation 10, using "calibration" parameters (see text). Shaded region indicates inert strength limit.

It is perhaps worth reiterating at this point that the curve fit procedure just described takes full cognizance of a residual driving force in the fracture mechanics. If we were to adopt the normal course in fatigue analysis and treat the indentation cracks as ideal Griffith flaws we would compute an entirely different curve. It might be argued, for instance, that since $c_0' > c_m$ in our experiments the crack front could be considered sufficiently far removed from the actual source of residual stress for the system to be effectively dominated by the applied loading field. A test of this argument is to measure n' from a data fit to Equation 11: as indicated in Section 2.2, the prediction for Griffith flaws is $n' = n = 17.9 \pm 0.5$; the corresponding prediction for flaws under the full influence of a residual stress term (i.e. for $c_0' < c_m$) is, from Equation 12, $n' = n/2 + 1 = 10.0 \pm 0.3$. An actual least squares fit to the data shown in Fig. 2 gives $n' = 10.2 \pm 0.3$. It is clear that the residual stress effect is far from insignificant here.

5. Discussion

We have indicated that residual-contact terms can play a large role in the mechanics of line-flaw growth to failure. In particular, crack velocity exponents as estimated from slopes of fatigue plots can be in error by as much as a factor of two if such residual terms are omitted from the analysis. This factor is considerably greater than that for the corresponding point-flaw case [1], reflecting the greater range of influence of the residual stress intensity factor K_r in the line-flaw geometry [6]. Bearing in mind the key position occupied by crack velocity exponents in modern-day lifetime design schemes for brittle components [18, 19] it would seem reasonable to advocate more attention to characterization of strength-controlling flaws, especially in regard to their local configurational stress history [20]. In cases where direct observation of critical flaw evolution proves impractical during the actual failure testing, some alternative means of quantifying the residual stress effect, e.g. by comparing inert strengths for flaws in their as-produced and re-annealed states (Section 3.2), would appear desirable.

The results described above have important implications concerning the lifetime properties of ceramics whose surfaces have been finished by a contact-induced process, especially by machining.

Machining damage may be regarded in terms of a high density accumulation of near-linear flaws. Generally, the critical, strength-degrading member of this accumulated population will experience a somewhat reduced residual crack driving force relative to that for an isolated median crack. For, in addition to the several relaxation factors mentioned in Section 2.1 in relation to the validity of Equation 2, neighbouring damage tracks will interact via their elastic/plastic fields so as to impose a countervailing, crack closure stress at the reference flaw [21]. Moreover, the enhanced lateral-crack chipping which facilitates the machining process might be expected to lead to physical removal of the deformation zone at the mouth of this flaw, and thereby of the very source of the residual field. Recent detailed investigations of machining damage in hot-pressed silicon nitride by Marshall [22] have nevertheless demonstrated that residual contact stresses can still play a dominant role in the failure mechanics. Indeed, in Marshall's strength experiments, conducted under effectively inert testing conditions, the critical median flaw always showed substantial precursor growth prior to reaching instability (i.e. $c_0' < c_m$, in the terminology of Section 2); the silicon nitride thus appears to be less influenced by residual-field relaxation processes than does our glass, presumably due to a relatively strong immunity to environmental slow crack growth effects. In this context it may be pointed out that much of present day ceramics strength analysis is carried out on test pieces with machined surfaces, in conjunction with conventional fatigue theory. It is clear now that crack velocity parameters obtained from this approach will generally not match those measured in macroscopic-crack test pieces [13], and, as such, will not provide a sound basis for lifetime design, particularly if the predictions involve extensive extrapolations beyond the data range.

Although the line-flaw test procedure described in this work is useful for emphasizing the importance of residual-stress terms in flaw micromechanics it suffers certain disadvantages, particularly in comparison with its point-flaw counterpart, as an avenue to routine materials evaluation. For a start, the median flaws remain subsurface along their length, and are therefore not amenable to optical examination in the simple manner of radial cracks at Vickers impressions. We have also noted that the growth of the line flaws tends to be somewhat erratic. Again, it would appear that line flaws are more susceptible to processes which partially relax the residual contact field, thereby leading to violation of the proviso $c_0' < c_m$ for validity of the closed-form fatigue solutions Equations 12 and 13.

Appendix I: Equivalence relations between normal-line and sliding-point loading

In this Appendix we investigate the connecting relation for the "effective" line force in two, essentially equaivalent, contact configurations: (i) wedge loading, at actual normal contact load P_l per unit length; (ii) axisymmetric loading, at normal contact load P but with linear translation.

To obtain the correspondence between the two cases we define hardness parameters in terms of the mean contact pressures:

$$H_l = P_l/2a \qquad \text{(line)} \qquad \text{(A1a)}$$

$$H = P/\alpha a^2 \qquad \text{(point)} \qquad \text{(A1b)}$$

where α is a geometrical constant of the point indenter. The condition for equivalence is that the track half-widths a should be identical in Equations A1a and A1b, i.e.

$$P_l = [2H_l/(\alpha H)^{1/2}]P^{1/2}. \qquad \text{(A2)}$$

Then insofar as the hardness parameters can be regarded as load invariant, which generally requires that the indenters should be of fixed profile (thereby preserving geometrical similarity) [23], we may use Equation A2 to evaluate the effective line force generated in translating-point contact.

We may note that the essence of this result, that $P_l \propto P^{1/2}$, is not addressed in the present experimental study, since all data are obtained at a single load $P = 5$ N.

Appendix II: Elastic/plastic analysis of residual line-contact field

Here we derive an expression for the dimensionless material/indenter parameter χ in Equation 1 of the main text, in terms of elastic/plastic properties of the material and the half-angle ϕ of the indenter. To do this we proceed exactly as for the point-contact configuration described in [9], simply replacing the model of an expanding spherical cavity used there with an analogous expanding cylindrical cavity, as appropriate to the plane-strain deformation geometry in Fig. 1.

Thus, we suppose that the plastic zone beneath the linear track may be considered to be of

circular cross-section, radius b. The residual force field associated with the formation of this zone may be estimated by the following hypothetical cut, operate and heal sequence:

(i) Starting with the original, unstressed elastic half-space, remove a cylindrical segment of radius b about the contact centre line.

(ii) Plastically deform the removed segment over the ultimate contact area to produce a characteristic line impression of half-width a, such that the plastic strain is accommodated as an outward radial displacement at the cylinder surface. Then, ignoring any depth recovery during unloading of the indenter [24], so that we may equate the impression depth to $a \cot \phi$, we obtain for the configurational bulk strain of the zone

$$\delta V/V \propto (a^2 \cot \phi)/b^2. \qquad \text{(B1)}$$

(iii) Restore elastically the segment to its original radius by applying a hydrostatic pressure across the cylindrical boundary,

$$p_b \propto \kappa(\delta V/V) \propto E(a/b)^2 \cot \phi \qquad \text{(B2)}$$

where in converting from bulk modulus κ to Young's modulus E we have omitted terms in Poisson's ratio.

(iv) Restore the cylinder to its original cavity in the half-space, allow the interface to heal, and allow the system to relax elastically. The cylinder will then exert an outward pressure on the encasing matrix. In the far-field approximation $c \gg b$ this pressure will be manifest as a residual mouth-opening line force

$$P_r \propto p_b b \propto [(a/b)(E/H_l) \cot \phi] P_l \qquad \text{(B3)}$$

where we have invoked Equation A1a to eliminate a in favour of P_l.

To proceed beyond this point we need to determine the dependence of the elastic/plastic cavity parameter a/b on material/indenter properties. For this we make recourse to Hill's analysis for the axially symmetric cylindrical problem [25]. His analysis provides an approximate normalized relation for the outward pressure p_0 acting on the internal cavity wall of radius r_0,

$$p_0/E = [1 + \ln (b/r_0)^2]/[(5 - 4\nu)(b/r_0)^2]. \qquad \text{(B4)}$$

A plot of Equation B4 is shown, for Poisson's ratio $\nu = 0.25$, as the solid curve in Fig. B1. Over a greater part of the range of b/r_0 covered this function may be approximated by the dashed line

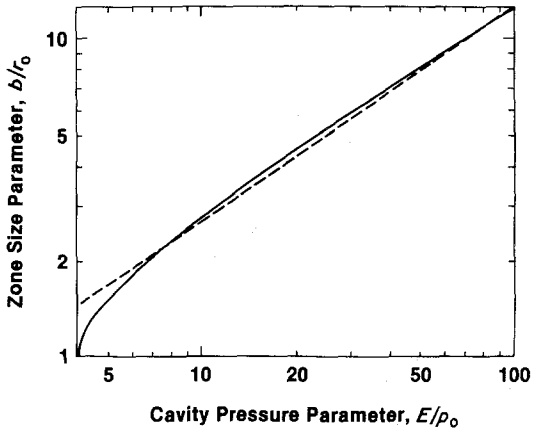

Figure B1 Plot of Equation B4, solid curve, and its power-law approximation, dashed line.

representation, which corresponds to a simple power-law relation

$$b/r_0 \propto (E/p_0)^m, \qquad \text{(B5)}$$

where $m \approx 2/3$. If now we identify the internal pressure with the appropriate hardness parameter, $p_0 = H_l$, and equate the volume of the cavity with the volume of the wedge impression, $a \cot^2 \phi = \pi r_0^2$, we have

$$b/a \propto (E/H_l)^{2/3} (\cot \phi)^{1/2} \qquad \text{(B6)}$$

The results from the expanding cylindrical cavity analysis are, in the far-field approximation considered here, pertinent to a straight-fronted crack of depth c loaded at its mouth by a concentrated line force P_r. The stress intensity factor for such a crack is of the form $K_r \propto P_r/c^{1/2}$ so, combining Equations B3 and B6, we obtain the required result for the master parameter in Equation 1 [9],

$$\chi = \xi (E/H_l)^{1/3} (\cot \phi)^{1/2} \qquad \text{(B7)}$$

where ξ is a further dimensionless constant, but one which is independent of material or indenter properties.

Acknowledgements

The authors wish to thank D. B. Marshall for valuable discussions on this work. Funding was provided in part by the Australian Research Grants Committee and by the United States Office of Naval Research.

References

1. D. B. MARSHALL and B. R. LAWN, *J. Amer. Ceram. Soc.* **63** (1980) 532.

2. P. CHANTIKUL, B. R. LAWN and D. B. MARSHALL, *ibid.* **64** (1981) 322.
3. B. R. LAWN, D. B. MARSHALL, G. R. ANSTIS and T. P. DABBS, *J. Mater. Sci.* **16** (1981) 2846.
4. R. F. COOK, B. R. LAWN and G. R. ANSTIS, *ibid.* **17** (1982) 1108.
5. T. P. DABBS, B. R. LAWN and P. L. KELLY, *Phys. Chem. Glasses* **23** (1982) 58.
6. E. R. FULLER, B. R. LAWN and R. F. COOK, *J. Amer. Ceram. Soc.* in press.
7. D. B. MARSHALL and B. R. LAWN, *J. Mater. Sci.* **14** (1979) 2001.
8. D. B. MARSHALL, B. R. LAWN and P. CHANTIKUL, *ibid.* **14** (1979) 2225.
9. B. R. LAWN, A. G. EVANS and D. B. MARSHALL, *J. Amer. Ceram. Soc.* **63** (1980) 574.
10. D. B. MARSHALL and B. R. LAWN, *ibid.* **64** (1981) C-7.
11. S. M. WIEDERHORN and B. R. LAWN, *ibid.* **62** (1979) 66.
12. M. V. SWAIN, *Proc. Roy. Soc. Lond.* **A366** (1979) 575.
13. B. J. PLETKA and S. M. WIEDERHORN, *J. Mater. Sci.* **17** (1982) 1247.
14. M. V. SWAIN, *J. Non-Cryst. Solids* **38–39** (1980) 445.
15. S. P. TIMOSHENKO and J. N. GOODIER, "Theory of Elasticity" (McGraw-Hill, New York, 1970) Chap. 4 and 13.
16. B. R. LAWN, D. B. MARSHALL and P. CHANTIKUL, *J. Mater. Sci.* **16** (1981) 1769.
17. G. R. ANSTIS, P. CHANTIKUL, B. R. LAWN and D. B. MARSHALL, *J. Amer. Ceram. Soc.* **64** (1981) 533.
18. J. E. RITTER, in "Fracture Mechanics of Ceramics" Vol. 4, edited by R. C. Bradt, D. P. H. Hasselman and F. F. Lange (Plenum, New York, 1978) p. 667.
19. S. M. WIEDERHORN and J. E. RITTER, in "Fracture Mechanics Applied to Brittle Materials", ASTM Special Technical Publication 678, edited by S. W. Freiman (ASTM, Philadelphia, 1979) p. 202.
20. B. R. LAWN and T. R. WILSHAW, "Fracture of Brittle Solids" (Cambridge University Press, London, 1975) Chap. 2.
21. R. F. COOK, B. R. LAWN, T. P. DABBS and P. CHANTIKUL, *J. Amer. Ceram. Soc.* **64** (1981) C-122.
22. D. B. MARSHALL, unpublished work (1982).
23. D. TABOR, "Hardness of Metals" (Clarendon Press, Oxford, 1951).
24. B. R. LAWN and V. R. HOWES, *J. Mater. Sci.* **16** (1981) 2745.
25. R. HILL, "The Mathematical Theory of Plasticity" (Oxford University Press, London, 1950) Chap. 5.

Received 6 September
and accepted 20 September 1982